

Alma Mater Studiorum Università di Bologna  
Archivio istituzionale della ricerca

Adhesion between SRP and masonry: Laboratory simulations of the field moisture and salt conditions

This is the final peer-reviewed author's accepted manuscript (postprint) of the following publication:

*Published Version:*

Gentilini C., Yuan Y., Carloni C., Franzoni E. (2020). Adhesion between SRP and masonry: Laboratory simulations of the field moisture and salt conditions. CONSTRUCTION AND BUILDING MATERIALS, 264(20 December 2020), 1-13 [10.1016/j.conbuildmat.2020.120697].

*Availability:*

This version is available at: <https://hdl.handle.net/11585/805815> since: 2021-02-27

*Published:*

DOI: <http://doi.org/10.1016/j.conbuildmat.2020.120697>

*Terms of use:*

Some rights reserved. The terms and conditions for the reuse of this version of the manuscript are specified in the publishing policy. For all terms of use and more information see the publisher's website.

This item was downloaded from IRIS Università di Bologna (<https://cris.unibo.it/>).  
When citing, please refer to the published version.

(Article begins on next page)

This is the final peer-reviewed accepted manuscript of:

**Cristina Gentilini, Yu Yuan, Christian Carloni, Elisa Franzoni, Adhesion between SRP and masonry: Laboratory simulations of the field moisture and salt conditions, Construction and Building Materials, Volume 264, 2020, 120697, ISSN 0950-0618.**

The final published version is available online at:

<https://doi.org/10.1016/j.conbuildmat.2020.120697>

#### Terms of use:

Some rights reserved. The terms and conditions for the reuse of this version of the manuscript are specified in the publishing policy. For all terms of use and more information see the publisher's website.

*This item was downloaded from IRIS Università di Bologna (<https://cris.unibo.it/>)*

***When citing, please refer to the published version.***

# Adhesion between SRP and masonry: laboratory simulations of the field moisture and salt conditions

Cristina Gentilini<sup>1a</sup>, Yu Yuan<sup>2b</sup>, Christian Carloni<sup>3c</sup>, Elisa Franzoni<sup>4b\*</sup>

<sup>a</sup>DA – Department of Architecture, University of Bologna, Viale del Risorgimento 2, 40136  
Bologna, Italy

<sup>b</sup>DICAM – Department of Civil, Chemical, Environmental and Materials Engineering, University of  
Bologna, Via Terracini 28, 40131 Bologna, Italy

<sup>c</sup>Department of Civil Engineering, Case Western Reserve University, 10900 Euclid Ave, Cleveland  
OH 44106, United States

<sup>1</sup>cristina.gentilini@unibo.it, <sup>2</sup>yu.yuan@studio.unibo.it, <sup>3</sup>cxc966@case.edu,

<sup>4\*</sup>elisa.franzoni@unibo.it (corresponding author)

Keywords: SRP, Masonry, Bond behavior, Moisture, Salt, DIC, Pull-off, Crystallization cycles, Shear test

**Abstract.** Steel-reinforced polymer (SRP) composites are a new addition to the fiber-reinforced polymer (FRP) composite toolbox for structural strengthening. While several authors investigated the bond behavior of SRP composites applied to a masonry substrate, little is known about the role played by the presence of moisture and salt in the wall. This study aims at investigating the bond behavior of SRP-masonry joints under two conditions: *i*) SRP strips are applied to masonry blocks that have been previously subjected to an artificial weathering protocol consisting in salt crystallization cycles; *ii*) SRP strips are applied to masonry blocks, and then the SRP/masonry joints are saturated with water. Single-lap shear tests are conducted on the SRP-masonry joints that underwent those two conditions. Digital image correlation (DIC) is used to obtain the strain on the surface of the SRP strips. The distribution of salts in the masonry blocks and at the SRP-masonry interface after failure

are investigated as well. Finally, the tensile strength of brick tested in both dry and saturated conditions is determined and compared.

## **1. Introduction**

It is well-known that masonry is the most common building material for load-bearing structures worldwide, but its low resistance to seismic forces makes strengthening interventions necessary [1]. Over last three decades, externally bonded (EB) fiber-reinforced polymer (FRP) composites have become a valuable technique, as they exhibit a high strength-to-weight ratio, are easy to apply and are versatile for different applications [2]. In recent years, twisted high-strength steel cords, typically arranged in unidirectional sheets, emerged as a new type of fiber for FRP composites. When steel fibers are employed, the FRP composite is known as steel-reinforced polymer (SRP) composite. A few publications have focused on SRP and have demonstrated the effectiveness of this strengthening system [3]. SRP composites are appealing because of the low cost of the fibers with respect to carbon and glass fibers, and the possibility of bending the fibers without chamfering the edges of the structure to which they are applied [4]. Moreover, steel cords allow to overcome the lack of ductility of carbon and glass fibers, as steel has some inherent ductility [5]. Steel cords also allow some mechanical interlock between the cords and the matrix, thus improving their bond [5].

The majority of studies that focus on strengthening applications with EB composites (both FRP and SRP) indicate that bond performance is a key aspect, since premature failure usually occurs due to the detachment of the composite from the substrate prior to the exploitation of the full load-sharing capacity of the composite. The bond behavior of SRP applied to brick or masonry samples has been studied by several researchers [6, 7]. Some authors focused on the durability of FRP-strengthened masonry and addressed the influence of moisture by investigating both material properties and bond behavior after prolonged water immersion [8, 9]. Other studies investigated the durability of FRP-strengthened masonry subjected to long-term exposure to high temperature [10] or salt crystallization [11, 12]. However, the experimental tests on the bond behavior of composite-masonry joints are

usually carried out using commercially-available fired-clay bricks. The bond behavior of FRP composites applied to an existing masonry substrate has received less attention in laboratory studies so far, although this is a crucial aspect for the performance of the reinforcement. Some authors [13-15] investigated the bond between FRP and historic bricks collected from historical buildings and observed that the failure mechanisms are influenced by the characteristics of the bricks, and in particular their compressive strength, porosity, chemical composition, and surface conditions. These studies suggest that historical masonry might behave differently from masonry constructed with current commercially-available bricks. Thus, there is a need of studying the effectiveness of the strengthening system applied to masonry that is built with actual historical bricks in order to simulate a masonry substrate similar to the real conditions in the field. However, the heterogeneity of the bricks collected from real buildings often leads to scattered experimental results, which are also attributed to different degrees of deterioration in bricks, different loading histories and different locations within the structure they are removed from. Employing artificially weathered masonry specimens to mimic in laboratory real conditions of masonry affected by rising damp and salt efflorescence could be an alternative approach to determine the response of strengthened masonry in the field, when subjected to a similar scenario. This approach was applied so far in the study of fiber-reinforced cementitious matrix (FRCM) composites [16, 17], and in a preliminary study on SRP composites [18].

The aim of this study is to investigate the bond behavior of SRP-masonry joints considering the effects of water and salts that may be present in actual field applications. In a first group of specimens, SRP composites are applied to masonry blocks that have been previously subjected to an accelerated weathering protocol, designed in a previous study [17], that induces salt crystallization through wet and dry cycles. In a second group of specimens, SRP composites are applied to unweathered masonry blocks and, after the SRP strips have been cured, the SRP-masonry joints are tested in water-saturated conditions. A third group of SRP-masonry joints is not weathered and tested in dry conditions as control. Direct-shear tests are conducted to determine the bond behavior in terms of failure modes and applied load-loaded end slip response. Digital image correlation (DIC) is employed to measure

the displacement field on the SRP surface and obtain the strain components on its plane. The salt amount and distribution in salt-laden specimens are obtained from ion chromatography analysis, which helps interpreting the results of the direct-shear tests. While direct-shear tests focus on the Mode-II fracture mechanics bond behavior (sliding), pull-off tests are also carried out to investigate the Mode-I bond (peeling) between resin and brick, under the same condition of the samples investigated in the direct-shear tests. Finally, to further understand the role played by water in the failure of bricks (which also influences the debonding mechanism), supplementary mechanical tests are performed on dry and water saturated bricks, namely three-point bending tests and tensile splitting tests. The aim of these additional test was not the investigation of the variation of the physical properties that characterize bricks in historic masonry, but the evaluation if some detrimental effect caused by moisture presence in bricks is present and may have an impact on the bond performance of the composite.

## **2. Materials and methods**

### *2.1 Materials and specimens*

The masonry blocks used in this study were built with six half solid fired-clay bricks ( $55 \times 120 \times 125 \text{ mm}^3$ ) and five 10 mm-thick mortar joints. Half bricks were obtained by sawing whole bricks. The cut faces of the bricks were placed on the same side of the block, which was not used to apply the SRP strip. L-shaped wood elements were placed at the corners of the masonry blocks to accommodate the straps used to tighten the blocks, which were necessary (Fig. 1) in order to guarantee a better maneuverability of the blocks. Their compressive strength (determined according to EN 772-1 [19]), tensile splitting strength (determined according to EN 12390-6 [20]), and elastic modulus with the corresponding coefficient of variation (CoV) resulted equal to 18.7 MPa (CoV = 2.0%), 1.6 MPa (CoV = 14.9%), and 6.2 GPa (CoV = 11.5%), respectively. According to technical data provided by the manufacturer, bricks also exhibit water absorption equal to 22%, lowest class of salts content (S2) and highest class of frost resistance (F2) according to EN 771-1 [21], adhesion strength 0.128

N/mm<sup>2</sup> (in plane initial shear strength of horizontal bed joints in masonry, according to EN 1052-3 [22]). The solid fired-clay bricks used for the blocks exhibit characteristics similar to those that can be commonly found in actual masonry structures, In fact, they were manufactured by pressing rather than extrusion (which is typical of industrial bricks). In addition, their mechanical and microstructural properties fall in the range of values reported for historic buildings, although identifying “typical” values is difficult due to the strong heterogeneity of pre-industrial bricks [23]. The compressive strength of historical bricks has been reported to be on average  $10.8 \pm 5.8$  MPa in a number of investigated buildings in St. Petersburg, Russia [24], 10.3 MPa in Istanbul, Turkey [25], 11.3 MPa (mostly in the range 2-22 MPa) in Venice, Italy [26], in the range 7-25 MPa in Riga, Latvia [27], and 23 MPa, 30 MPa and 23.5 MPa in different buildings investigated in Italy [28-29]. The mean water absorption value of historical bricks, measured directly or calculated on the basis of open porosity and bulk density values, was reported to be 18-20% in buildings of Henan province [30], 21% in Istanbul [25], 17.7-22.9% in Thailand [31], 15-30% in different buildings in Greece and Turkey [32], 15-29% in Italy [23].

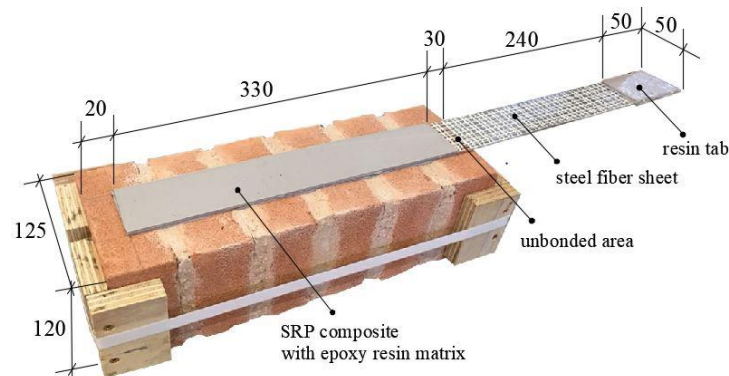


**Fig. 1.** Configuration and main dimensions [in mm] of the SRP-masonry joints.

A commercially-available dry-mix mortar with natural hydraulic lime binder was used for the masonry joints (class M5 according to EN 998-2 [33]).

Twelve masonry blocks were manufactured and cured for two months in laboratory conditions. The blocks were then divided into three groups:

- four masonry blocks were subjected to artificial weathering in saline solution prior to applying the SRP composite, and were labeled POST, which stands for post-weathering strengthening. This group of specimens was used to investigate the behavior of the composite when applied to a deteriorated masonry substrate. The artificial weathering procedure is described in details in [17]. In brief, each masonry block underwent 6 cycles, each of them consisting of two phases: 1) a wet phase, in which blocks were wrapped with duct tape on the lateral surface and partially immersed in a saline solution (sodium chloride 4 wt% and sodium sulfate decahydrate 10 wt%, solution head 20 mm) for 48 hours. Saturation was achieved by capillary rise; 2) a dry phase, in which the blocks were dried in a ventilated oven at 40 °C for 48 hours. Duct tape was used in an attempt to hinder lateral evaporation and promote vertical flow of the solution and the accumulation of salts on the top surface, where the SRP composite would have been eventually applied. Previous tests demonstrated that this weathering procedure can produce a salt accumulation similar to that found in actual buildings [12]. After the last drying phase, POST masonry blocks were strengthened with the SRP composite strips as described below. Single-lap shear tests on the SRP-masonry joints were conducted in dry conditions, as described below;
- four masonry blocks were not subjected to any weathering and were strengthened with SRP composite strips. These SRP-masonry joints were partially immersed in deionized water for the first 24 hours, by placing the lateral face in water in order to allow the air to exit from the pores of masonry during capillary absorption (otherwise the composite strips could prevent a complete degassing of masonry, due to its impermeable nature), and then totally immersed for additional 24 hours, to reach saturation. Direct-shear tests on these SRP-masonry joints were carried out in saturated conditions and these specimens were labeled SATU. The aim of this second group of specimens was to test the bond behavior of the SRP composite in actual masonry structures that can be in water-saturated or partially-saturated



condition during their lifetime (a common occurrence in historical masonry [34], possibly exacerbated by the presence of impermeable composite strips on the surface);

- four masonry blocks were not subjected to any weathering (labeled REF specimens), were strengthened with SRP composite strips, and were used for direct-shear tests after they were placed in the oven at 60 °C up to constant mass and left to cool in lab conditions prior to testing, for comparison. This specimen condition is referred to hereinafter as ‘dry’.

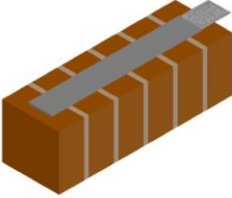
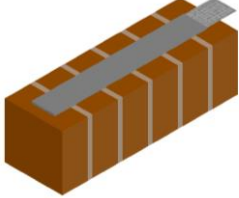
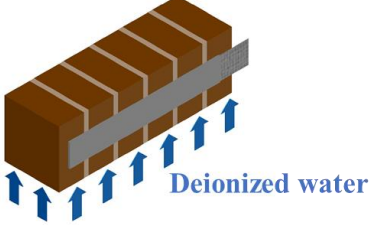
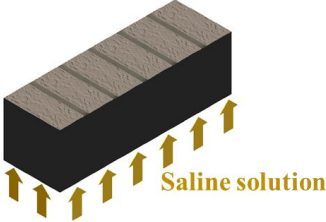
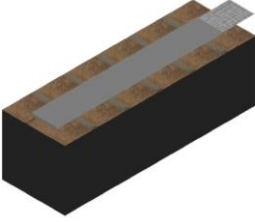
The composite material used in this study consisted of steel fibers embedded in a bi-component epoxy resin matrix. The epoxy resin exhibits tensile strength  $\geq 14 \text{ N/mm}^2$ , shear strength  $> 20 \text{ N/mm}^2$ , glass transition temperature  $+60^\circ\text{C}$ , pot life 75 minutes, Young’s modulus  $E > 5300 \text{ N/mm}^2$ , as reported in the manufacturer data sheet [35]. The steel fibers were ultra-high strength galvanized steel cords arranged as a unidirectional sheet fixed to a fiberglass micromesh to facilitate installation. The mass density of the steel sheet is  $1200 \text{ g/m}^2$ , while the cross-sectional area of the cord is  $0.538 \text{ mm}^2$  [36].

The SRP composite, which had a total nominal thickness equal to 4 mm, was applied to the masonry blocks as shown in Fig. 1. The fibers were embedded in the epoxy resin only in the bonded region. The bonded area started 30 mm from the edge of the masonry block in the direction of the applied load, to avoid premature spalling at edge of the block. At the end of the steel fiber sheet, resin tabs were cast to allow the jaws of the testing machine to grip the strip and effectively transfer the load. The procedure followed to apply the composite to the masonry blocks was comprised of the steps below:

- (for POST masonry blocks only) removal of efflorescence and detached parts from the surface by steel brush;
- cleaning off dust on the surface by means of an air blower;
- application of a first 2 mm-thick layer of resin on the clean surface. A plastic mold was used to define the bonded area;

- application of the steel fiber strip on the resin layer. To ensure that the cords were fully impregnated by the resin, a gentle pressure was exerted on the fiber sheet;
- application of a second 2 mm-thick layer of resin over the steel fiber sheet. Plastic molds were used to guarantee that the total thickness of the composite strip was 4 mm;
- demolding after the SRP strip cured for 24 hours;
- casting of a resin tab at the end of the steel fiber sheet.

A summary of the specimens and their testing conditions is provided in Fig. 2.

Group	Specimens preparation		Condition when tested
REF	 Application of SRP		Dry
SATU	 Application of SRP	 Saturation in deionized water	Saturated
POST	 Artificial weathering by salt crystallization cycles	 Drying, surface brushing and application of SRP	Dry

**Fig. 2.** Scheme of the preparation and conditions of specimens for single-lap shear tests (the arrows indicate the direction of capillary absorption).

## *2.2 Experimental methods*

### *2.2.1 Direct-shear test and subsequent materials characterization*

Single-lap shear tests were conducted in a classical push-pull configuration (Fig. 3), where the masonry block (after removing the wooden elements) was restrained in between two rigid plates connected by four bolted rods, while a tensile force was applied to the steel fiber sheet that was gripped by the jaws of a servo-hydraulic universal testing machine. Two linear variable differential transformers (LVDTs) were mounted on the masonry surface on each longitudinal side of the SRP strip near the loaded end. These two LVDTs reacted off of an aluminum  $\Omega$ -shaped plate, which was attached to the bare fibers close to the beginning of the bonded area. The average of the two LVDT measurements is defined as global slip,  $g$ , in this article. All tests were conducted at a global slip rate equal to  $0.84 \mu\text{m/s}$  until failure. Different shear tests to investigate the bond behavior of steel composites to masonry substrates are also available, as described in [37, 38].

For one specimen per each group, DIC was used to measure the displacement and obtain strain fields on the SRP and masonry surface. A speckle pattern was created on the region of interest, prior to testing, by applying a thin coat of white paint followed by random black dots obtained with spray paint. For SATU specimens, the speckle was created before immersion in water, since the application of the paint could be difficult on a wet surface. Two high-resolution cameras were employed to take images of the specimen during the test, and DIC 3D software was used to post-process the images.

After single-lap shear tests were performed, the fracture surface of the detached composite, possibly also including some adherent substrate, was observed in a stereo-optical microscope Olympus SZX10.

In order to investigate the amount and distribution of salts in the masonry blocks due to artificial weathering and to determine their influence on the bond behavior of the SRP composite, brick and mortar samples from two POST specimens were collected by chiseling them off, after shear tests were completed. For comparison, samples from a REF specimen were removed and analyzed as well. The sampling locations are shown in Fig. 4. Fragments of approximately 2-3 g were collected from

both bricks and mortar. The fragments were removed from two different locations along the longitudinal axis of the block: at the mid-length and almost at the end of the axis next to the free end of the composite (the latter is termed ‘end location’ for the sake of brevity). For each location along the axis of the masonry block, two samples were extracted: one beneath the surface of the masonry block (where the SRP was applied) and one close to the centroid of the cross-section. It should be pointed out that samples removed from beneath the surface were actually taken at a distance equal to 2-4 mm from the surface to avoid the presence of the efflorescence. In addition, the samples in all locations described above were taken from brick and mortar. Thus, eight fragments were collected and analyzed for each specimen. These samples were ground to powder ( $<0.075$  mm), put in deionized boiling water and filtered by filter paper, and then the soluble salt amount in terms of anions were determined by ion chromatography (Dionex ICS-1000).

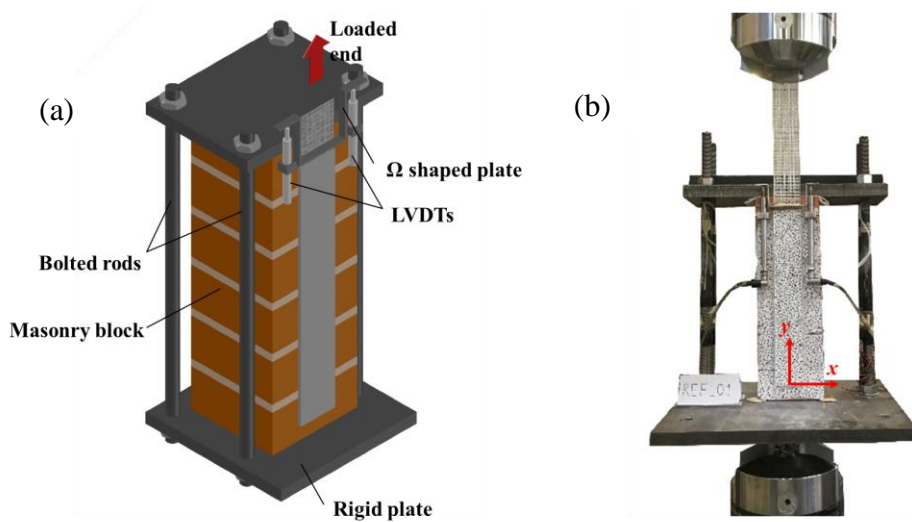


**Fig. 3.** Single-lap shear test: (a) 3-D sketch of the test set-up and (b) photo of specimen during the test with the speckle pattern for DIC (reference system is shown).

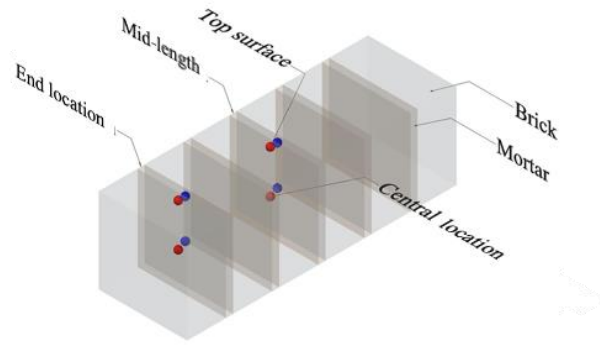


**Fig. 4.** Sampling locations for ion chromatography (brick fragments are represented in red and mortar fragments in blue). With respect to the longitudinal axis of the masonry block, samples were taken at mid-length and at the end. For both locations, samples were removed from brick and mortar beneath the surface of the block and close to the centroid of the cross-section.

#### 2.2.2 Pull-off test and other mechanical tests

Pull-off test is considered a simple and relatively inexpensive method to evaluate the quality of the adhesion between composite and substrate. Its procedure is described in EN 1542 [39]. Although the direction of the load applied in this test is different from that of the single-lap shear test, pull-off test is one of the few tests that can be performed on site with a limited destructive action [40]. Hence, in the present study this test was carried out with the aim of investigating whether its results can be at least qualitatively compared with those obtained from single-lap shear tests. The same type of SRP composite and six bricks taken from the same batch used for the construction of the masonry blocks were used. The composite was applied to the bed face of the bricks, following the same application procedure described above, and the same groups of specimens were constructed:

- two bricks were subjected to the same salt crystallization cycles described in Section 2.1. Then, the bricks were cleaned with a steel brush, strengthened with the SRP composite and tested in dry condition (POST specimens);
- two unweathered bricks were strengthened with the SRP composite and then water saturated (SATU specimens). These specimens were tested in saturated condition;
- two unweathered bricks were strengthened with the SRP composite and tested in dry condition (REF specimens).

The application of the composite on the bed face of the brick rather than on its side surface (which is the one actually reinforced on-site) may lead to considerably different results [41]. In this work, although the authors are aware of such issue, the strip was applied to the bed surface (only for pull-off tests). The main reason is that both the equipment for pull-off tests and the common size of the aluminum disc were too large to be applied on the bed surface, which is  $55 \times 120 \text{ mm}^2$ . It should be noted that the aluminum disc used in the pull-off test (Fig. 5b) had a diameter of 50 mm, which was considered sufficiently large (given the grain size of the material) to pull off a representative area of the composite and the brick underneath. In addition, the main goal of performing pull-off tests was to compare the results of the specimens tested in three different conditions (REF, SATU, and POST) and qualitatively compare the results with those of single-lap test specimens under the same three conditions. To carry out the pull-off tests, a circular groove (50 mm nominal diameter) was carved by using a core-drilling tool. The groove was 15 mm deep as the coring operation went through the composite surface (4-mm thick) and the substrate. For each SRP-strengthened brick, two circular grooves were cut (Fig. 5a). An aluminum disk (50 mm diameter) was glued on the composite surface with an epoxy adhesive (the same used for the composite matrix). During the pull-off test, the specimen was fixed to a rigid steel frame and tested by means of a portable pull-off device that applied a tensile force to the aluminum disk up to failure (i.e. complete pull-off of the disk). A load cell was also employed to check the load value. The pull-off test set-up is shown in Fig. 5b.

It is well-known that the mechanical properties of the substrate strongly influence the bond behavior of FRP composites [18], as cohesive failure usually occurs in the substrate rather than within the composite. In this study, the effect of the presence of moisture in masonry on the bond behavior of SRP composite was investigated by comparing SATU and REF specimens (employing the results of single-lap shear and pull-off tests). However, water can influence the mechanical behavior of porous materials such as bricks. Therefore, the presence of moisture might be affecting the substrate as well as the composite-brick interface.

The tensile splitting and flexural strengths of the brick in saturated and dry conditions were determined to investigate whether and to what extent water in the pores affects the mechanical properties of brick. To take into account the heterogeneity of bricks, specimens used in these additional tests were extracted directly from the bricks of the REF masonry blocks, after single-lap shear tests were completed. Fifteen  $30 \times 30 \times 120 \text{ mm}^3$  brick prisms were sawn for three-point bending tests and 24 cores (diameter 38 mm and height 38 mm) were core-drilled for splitting tensile tests, as shown in Fig. 6. Then, half of these samples was immersed in deionized water up to constant weight, while the other half was tested in dry condition.

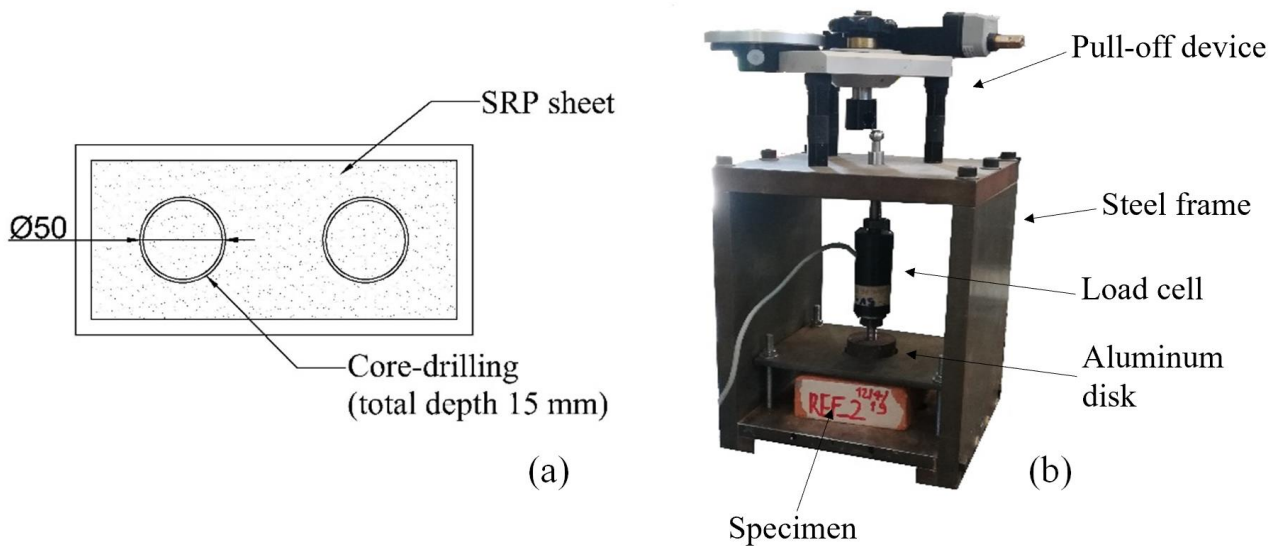


**Fig. 5.** Pull-off test: (a) top view of the brick with core-drilled grooves [dimensions in mm] and (b) photo of the specimen during the test.

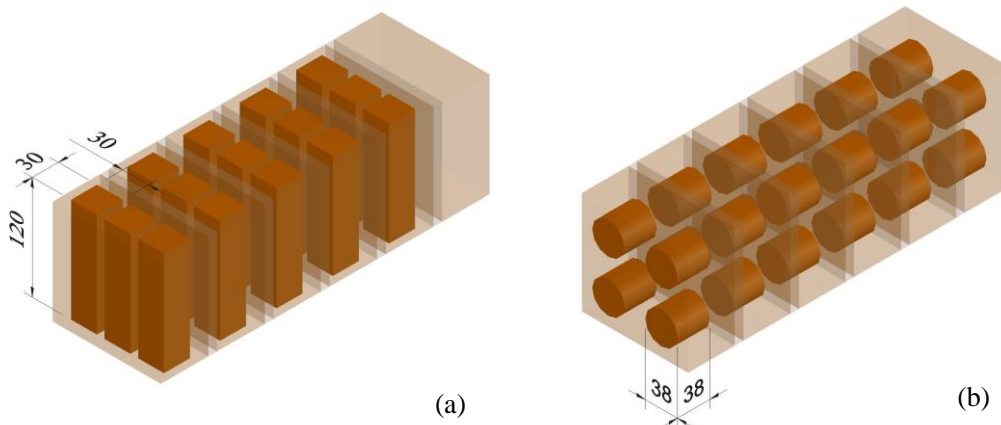


**Fig. 6.** Brick specimens extracted from REF masonry blocks for: (a) three-point bending tests and (b) tensile splitting tests [dimensions in mm].

### 3. Results and discussion

#### 3.1 Direct-shear test and subsequent materials characterization

The applied load versus global slip ( $P$ - $g$ ) curves for all single-lap test specimens are reported in Fig. 7, together with the corresponding failure modes, see also Fig. 8. The main mechanical parameters in terms of loads, average values as well as corresponding slips are collected in Table 1. For some specimens (REF\_02, SATU\_01 and POST\_04) complete detachment (debonding) of the SRP strip did not occur, due to local failure of the masonry block or to the detachment of the LVDTs. Thus, for these specimens the results in terms of  $P$ - $g$  curve were not considered. Regarding the failure modes, all REF specimens exhibited a cohesive failure (Fig. 7a and Fig. 8), characterized by the detachment of the SRP strip with a layer of masonry attached to it (about 3-5 mm thick). The attached layer was slightly thicker in the area corresponding to the mortar joints than that in the area of the interface corresponding to the brick. Among the possible reasons for a different thickness of the layer of mortar and brick, the authors have considered a deeper penetration of the resin into the mortar joints (because of a different porosity) or a change of the compliance between the SRP-brick and SRP-mortar interface. In SATU specimens (Fig. 7b), cohesive fracture was observed, but the layer of masonry still attached to the SRP strip was considerably thinner than the one observed in REF specimens. In POST specimens (Fig. 7c), a mixed failure mode was observed, which included an interlaminar failure within the SRP strip (i.e. slip of the fibers with respect to the matrix that resulted in a fracture along the fiber-internal layer of epoxy interface) and cohesive failure between SRP strip and masonry substrate with a thin (about 1-2 mm thick) layer of the substrate attached to the SRP strip. For POST\_02 specimen, the detached surface of the composite strip was smooth (i.e. with almost no substrate attached), except for the areas adjacent to the mortar joints, where a thin layer of brick and mortar remained attached to the composite, while towards the free end an interlaminar failure occurred and the bare fibers were visible.



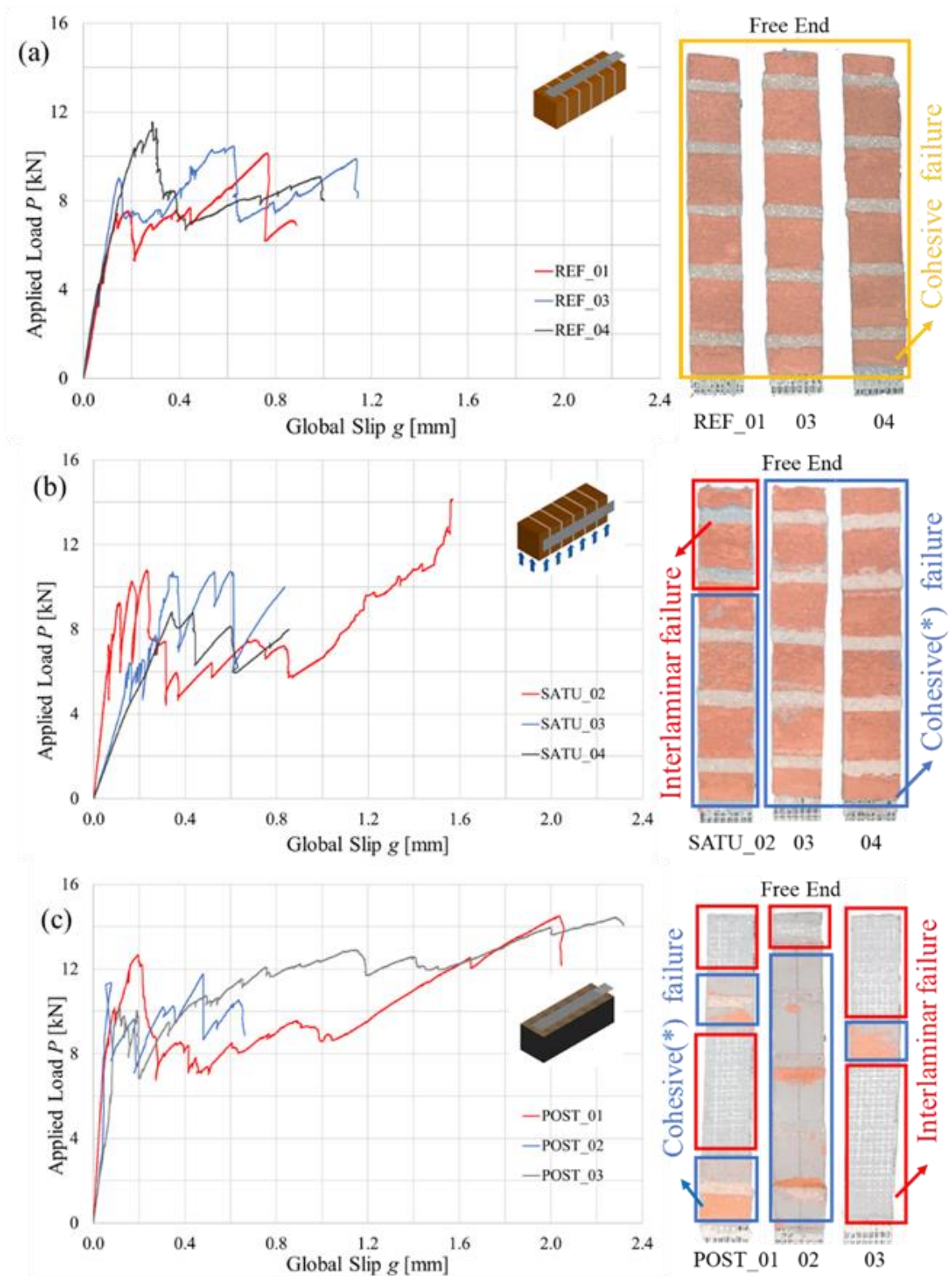


**Fig. 7.** Applied load  $P$  - global slip  $g$  curves and failure modes for (a) REF (b) SATU and (c) POST specimens.

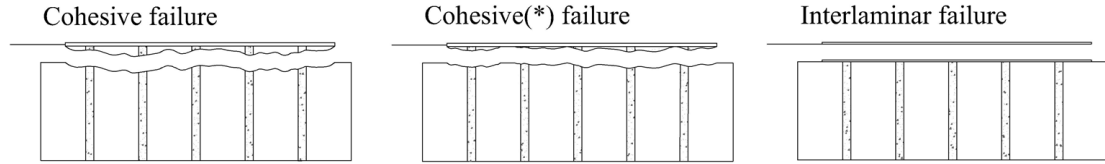


**Fig. 8.** Failure modes observed in direct-shear tests. ‘Cohesive failure’ mode refers to the detachment of a layer of the substrate with an average thickness equal to 4 mm; ‘Cohesive(\*) failure’ mode refers to the detachment of a layer of the substrate with an average thickness equal to 1 mm; and ‘Interlaminar failure’ mode refers to the detachment of the fibers at the interface with the internal layer of matrix.

**Table 1.** Results of the single-lap shear tests: load values and failure modes (CoV within parentheses).

Group	Specimen	First peak load [kN]	Corresponding slip [mm]	Maximum load [kN]	Corresponding slip [mm]	Failure mode
REF	REF_01	7.43	0.13	10.14	0.76	Cohesive
	REF_02	/	/	/	/	Cohesive
	REF_03	9.03	0.15	10.45	0.78	Cohesive
	REF_04	11.56	0.28	11.56	0.28	Cohesive
	Average	9.34 (22.3%)		10.72 (7.0%)		
SATU	SATU_01	/	/	/	/	Cohesive(*)
	SATU_02	9.25	0.11	14.16	1.69	Interlaminar and Cohesive (*)
	SATU_03	6.42	0.16	10.85	0.57	Cohesive (*)
	SATU_04	8.83	0.34	8.83	0.34	Cohesive (*)
	Average	8.17 (18.7%)		11.28 (23.9%)		
POST	POST_01	12.63	0.20	14.49	1.98	Interlaminar and Cohesive (*)
	POST_02	/	/	/	/	Cohesive(*)
	POST_03	10.20	0.12	14.44	2.54	Interlaminar and Cohesive (*)
	POST_04	/	/	/	/	Cohesive (*)
	Average	11.41 (15.1%)		14.47 (0.2%)		

All the  $P$ - $g$  curves show an initial linear portion followed by a non-linear behavior characterized by several load drops that in the case of REF specimens are clustered around load values between 8 and 10 kN, while for SATU group the average load values are between 6 and 8 kN. It should be noted that the last ascending branch that characterizes SATU\_02 specimen is due to a Mode I failure mode, that involved the detachment of a portion of a brick bulb towards the free end of the composite. This last part is not meaningful in terms of fracture mechanics Mode-II bond capacity, since it involves a Mode I failure [42, 43]. The lower load range for SATU specimens is most likely associated with the substrate properties in wet conditions. This aspect will be further investigated below. In POST specimens, results are more scattered due to the presence of salts in the substrate. On average, after the linear branch, the curves oscillate within load values between 8 and 10 kN as for REF specimens. As observed for the SATU\_02 specimen, the final ascending branch that is visible in POST\_01 and POST\_03 specimens is related to Mode I failure mode, involving the detachment of a thicker portion of substrate at the free end. For specimens characterized by a cohesive failure mode (i.e. REF and most of the SATU specimens), the load drops correspond to the engagement of the mortar joints in the fracture process [44]. The first peak load is associated with the engagement of the first mortar joint in the stress transfer at the interface. The cohesive composite-mortar interface is associated with a lower fracture energy and most likely smaller values of interfacial slip when compared with the composite-brick interface [45]. Thus, when and as long as the stress transfer engages the composite-mortar interface, the transferred load is lower than what it would be if only the composite-brick interface was engaged. For specimens with interlaminar fracture (POST specimens), it is difficult to determine whether the first peak load is associated with the engagement of the first mortar joint as slip between the SRP strip and substrate occurs, or a switch of interfaces and therefore slip between the fibers and the resin. It is possible that both interfaces are activated and additional tests would be necessary to determine the hierarchy of interfaces and their interaction. Under ideal conditions, the observed load drops should correspond to debonding that involved the mortar joints [46]. However, transversal cracks in the

resin were observed for POST specimens as interlaminar failure occurred for these specimens. A possible explanation of load range similar to the REF group can be associated to the presence of a mixed cohesive and interlaminar failure mode. However, this result may or may not be due to a better quality of the substrate (which was possibly deteriorated by salts) or to a better adhesion since cohesive failure with a very thin layer of substrate attached the composite strip was observed in portions of the debonded area. It should be noted that in field applications that deal with historical masonry structures, the bond behavior and, as a consequence, the failure mode, can be related not only to the substrate conditions (salt deterioration and moisture presence), but they may also be influenced by other factors, such as the possible presence of defects inside the SRP composite, the heterogeneity of historical hand-made masonry bricks, and the geometrical unevenness of historical masonry surface.

Comparing the slope of the initial linear part of the responses, SATU specimens exhibited a large scatter in the initial stiffness with the lowest values among all groups, which could be possibly ascribed to the presence of moisture in the substrate and/or to a possible misalignment of the LVDTs. This aspect will be investigated below with the comparison between DIC and LVDT measurements.

*P-g* curves obtained from LVDT and DIC measurements are compared in Fig. 9. The DIC curves were obtained by averaging the displacement component in the direction of the fibers in two small areas. One area was centered across the width of the SRP strip and located at the beginning of the bonded area at the loaded end. The second area was located on the masonry surface adjacent to the beginning of the bonded area. The global slip  $g$  was obtained by subtracting the average displacement of the second area from that of the first area. DIC and LVDT curves are in good agreement, in particular in the linear part. However, it should be noted that the slope of the linear branch for SATU\_02 specimen differs between that obtained from DIC with the one obtained from LVDT measurements. In particular, LVDT slope is steeper with respect to DIC, suggesting that the LVDT could have been mounted on the fibers closer to the bonded area with respect to the other ones, resulting in a stiffer response. A slight change in the location where the  $\Omega$ -shaped plate was mounted

could also explain the difference in slope of the linear branch of SATU\_02 specimen curve in Fig. 7b with respect to the other SATU specimens.

The fracture surface of all specimens was also observed by means of an optical microscope and the photos of some representative specimens are reported in Fig. 10. In REF specimens, the layer of brick and mortar that was left attached to the composite after complete debonding of the SRP strip can be observed in Fig. 10a. A much thinner layer of substrate (when compared with REF specimens) was detached along with the composite in SATU specimens (Fig. 10b). Figures 10c and 10d provide an interesting insight into the fracture surface of POST specimens. The portions of the bonded area that exhibited a cohesive failure with a thin layer of masonry attached suggest that adhesion between resin and brick was compromised by the weathering cycles. Even though the masonry surface was cleaned prior to applying the SRP strip, the substrate was probably deteriorated by the presence of micro-cracks caused by salt crystallization. The photos also show that, in the portions of the bonded area where interlaminar failure occurred, the steel fibers appeared clean (Figs. 10c and 10d). This might suggest a weak adhesion between resin and steel textile. The reason can be twofold: on one hand, air bubbles were observed within the polymeric matrix (Fig. 10d), possibly due to some unexpected factors, such as a too-long mixing, or a too-prolonged casting procedure in the manufacturing of the composite strip, or a too-high environmental temperature (in fact, bi-component epoxy resins are known to have a limited pot-life). On the other hand, even if the substrate was brushed from surface efflorescence, salts are still present and they may have retained water and humidity that could have played a detrimental action for a complete polymerization of the resin at the interface. However, additional tests would be necessary to understand why a different interface was activated. In particular, scanning electron microscope (SEM) could be used to observe the interface between the deteriorated brick and the composite matrix at different locations and Fourier-Transform Infrared Spectroscopy (FT-IR) performed on resin fragments collected from this interface could help evaluate whether polymerization was incomplete.

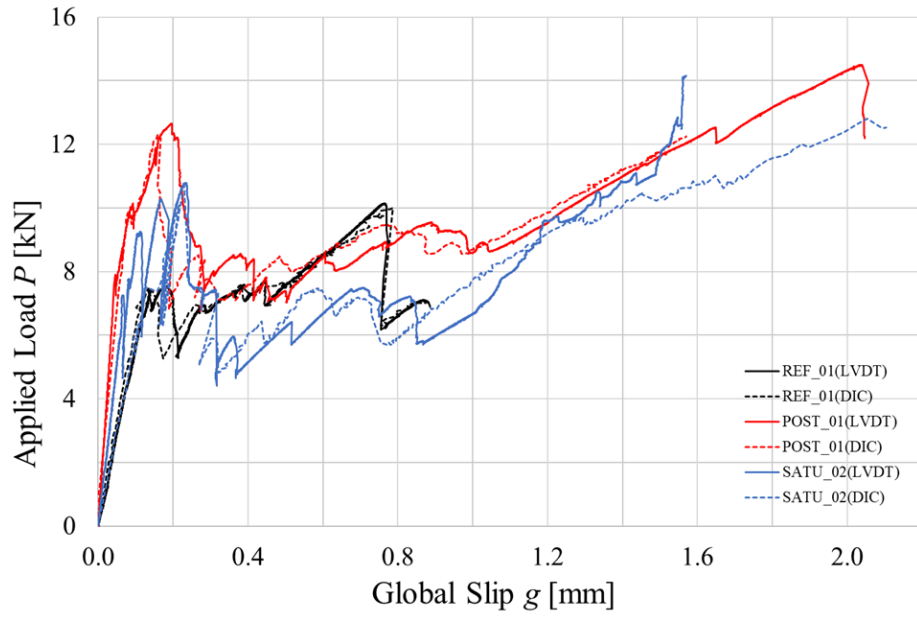


**Fig. 9.** Comparison of the  $P - g$  curves obtained from LVDT and DIC measurements.

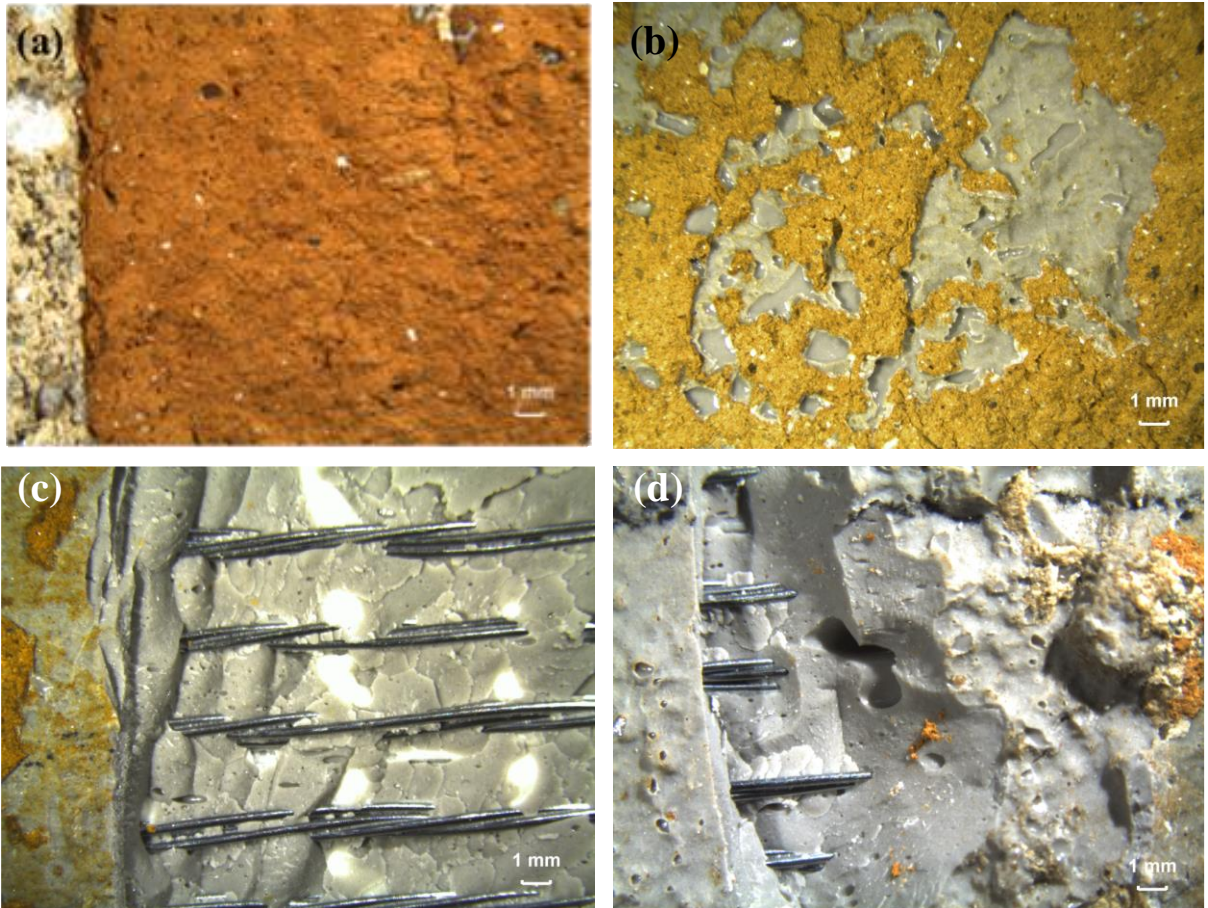


**Fig. 10.** Optical microscope photos of the debonding surface on the SRP composite: (a) REF; (b) SATU and (c)-(d) POST specimens.

To further discuss the stress transfer in SRP-masonry joints, profiles of the longitudinal strain component,  $\varepsilon_{yy}$ , along the central line of the SRP strip (reference system is shown in Fig. 3b) obtained from DIC analysis were considered. As a first approximation, strain on SRP surface can be considered representative of the strain at the composite-substrate interface [47-49]. Several points along the *P-g* curves were selected to plot the strain profile along the SRP strip. From the strain profiles reported in Fig. 11, the following observations can be made:



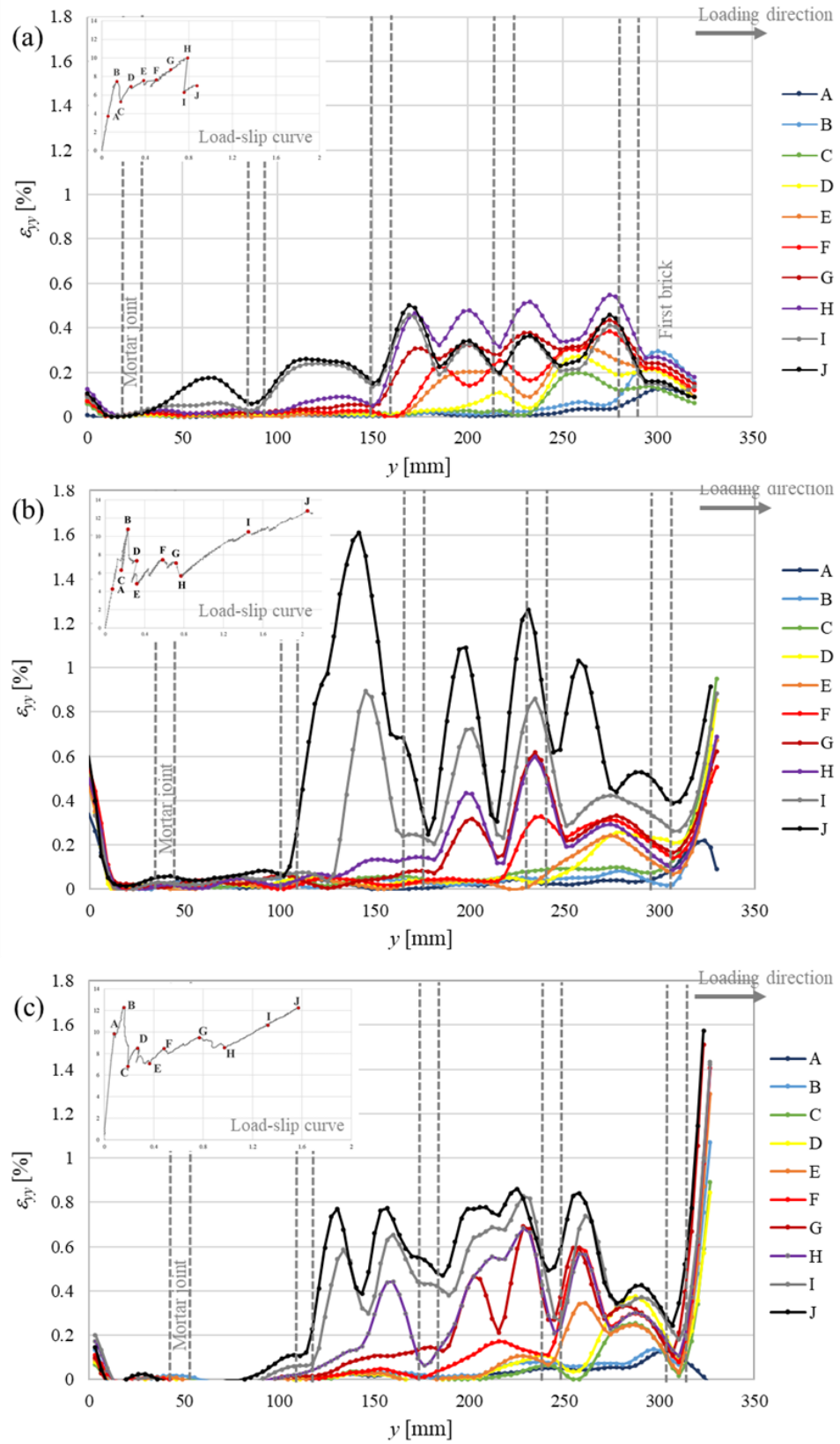


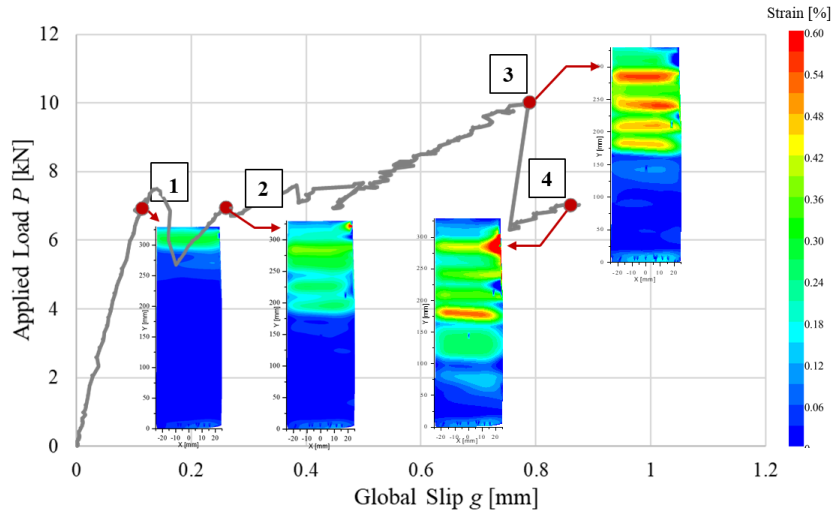
**Fig. 11.** Longitudinal strain profile along the central line of SRP composite for specimens (a) REF\_01, (b) SATU\_02 and (c) POST\_01.



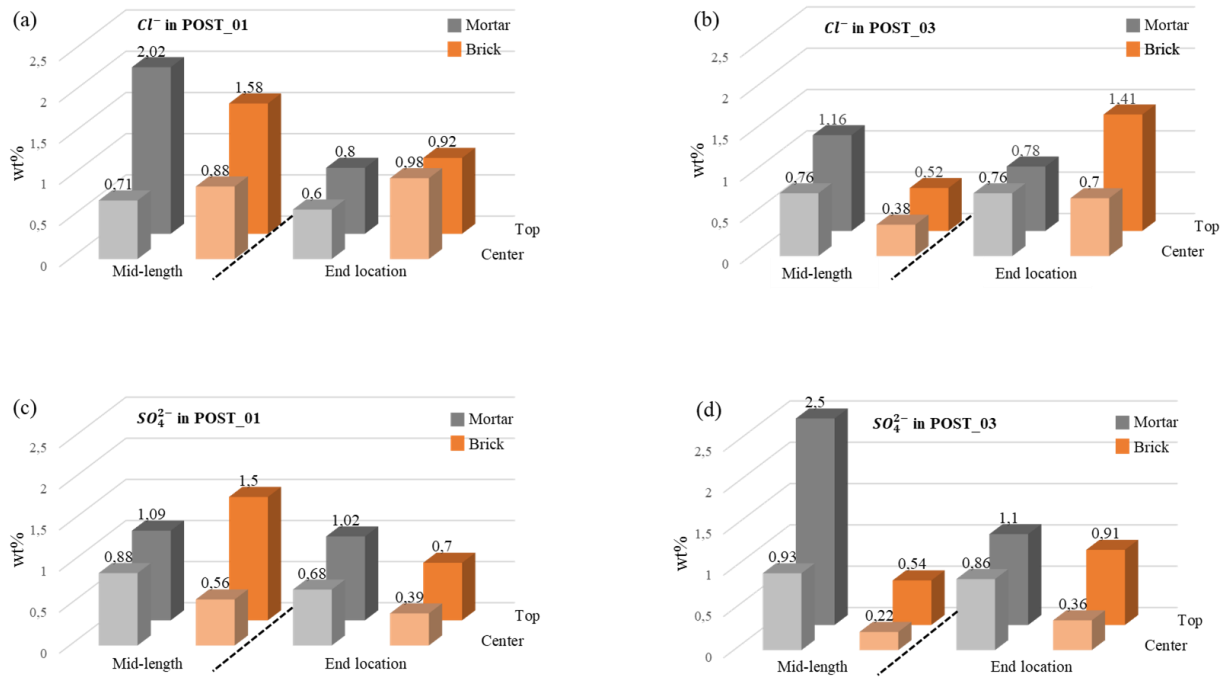
- in all groups, strain distribution is characterized by peaks that are mostly concentrated within the bricks, with higher values near the loaded end. These peaks suggest that the load transfer mainly takes place at the interface with bricks [49];
  - as global slip  $g$  increases, the strain profile fully develops and shifts towards the free end of the composite. For REF specimen (Fig. 11a) after the first peak load (point B), stress transfer takes place mainly in the first brick and then moves further along to the following one and then progressively to others, while debonding starts at the loaded end. The contour plots of the longitudinal strain component  $\varepsilon_{yy}$  over the SRP surface are shown in Fig. 12 for different load levels. The shift of the stress transfer from loaded end towards free end can be clearly observed;
  - for SATU\_02 specimen (Fig. 11b), after point H, the  $P$ - $g$  curve is characterized by a long ascending branch, which, as stated before, is related to Mode I failure mode. The corresponding strain profiles (curves H, I and J) are left for sake of completeness although they cannot be directly compared to the other strain curves related to Mode II failure mode.
- The same behavior can be observed in the POST\_01 specimen (Fig. 11c).

Figure 13 shows the amount of chloride and sulfate ions in two POST specimens (POST\_01 and POST\_03), while the amounts of salts in unweathered brick and mortar collected from REF specimens are reported in Table 2. The amount of salts was considerably increased by the artificial weathering process. Higher percentages of salts were found on the top surface (in the range 0.5-2.5%) with respect to the area near the centroid of the cross-section of the masonry blocks, and these amounts are consistent with the salts usually present in historical buildings [50, 51]. The distribution of salts on the top surface is very irregular, due to fact that the evaporation rate of saline solution may be different at different locations along the specimens due to several factors, which might have contributed to the irregularity of the applied load-global slip curves and failure modes of the direct-shear tests. Lower amounts (in the range 0.2-1.0%) and a more regular distribution of salts were found in the centroid of the cross-section of the blocks, where no evaporation took place. It can be concluded

that the adopted artificial weathering procedure allowed to obtain quite realistically deteriorated masonry blocks.



**Fig. 12.** Contour plots of strain component  $\varepsilon_{yy}$  on the surface of REF\_01 SRP strip at different load levels.



**Fig. 13.** Amount of chloride ions in (a) POST\_01, (b) POST\_03 and amount of sulfate ions in (c) POST\_01, (d) POST\_03 (sampling locations described in Fig. 4).

**Table 2.** Salts amounts in brick and mortar extracted from a REF specimen in the central locations.

Sample	Mortar		Brick	
	$Cl^-$ [wt%]	$SO_4^{2-}$ [wt%]	$Cl^-$ [wt%]	$SO_4^{2-}$ [wt%]
REF	0.05	0.16	0.04	0.18

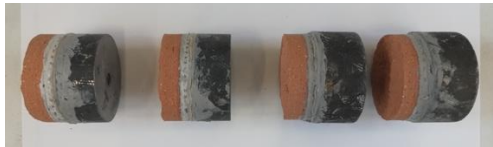


### 3.2 Pull-off test and other mechanical tests

The results of pull-off tests are reported in Table 3. Both REF and SATU specimens exhibited a neat cohesive failure, with a fracture surface that was located at 8-10 mm from the surface of the brick (corresponding to the bottom of the groove made by the drilling machine). The average strength of SATU specimens was slightly lower than that of REF specimens and this decrease could be due to a reduction of brick strength after water saturation (this aspect will be further investigated below). Specimens from the POST group exhibited a bond failure at the composite/weathered brick surface that resulted in an almost-cleaned surface. Consequently, for POST specimens a substantially low, almost negligible, average pull-off strength was observed. From a qualitative point of view, the results of pull-off tests and those obtained from direct-shear tests, although not fully comparable due to the different brick faces that were strengthened and to the presence of mortar joints in the masonry blocks used for shear tests, allow to make some remarks:

- a slight reduction in the bond performance due to water saturation of the substrate (SATU specimens), with respect to dry substrate, was observed in both tests, with a cohesive failure mode. In the pull-off tests, the layer of brick detached was thick, while in the shear test it was extremely thin;
- the salt deterioration of the substrate (POST specimens) might have altered the adhesion of the SRP to the masonry substrate. In the pull-off tests, POST group showed a clear trend with an almost negligible strength with respect to the other groups. In the shear tests, the trend in terms of debonding load is not so clear. In fact, the presence of the joints and the activation of multiple interfaces might have influenced

the results. In addition, it is possible that the presence of salts might have negatively affected the properties of Mode-I, which is inherently present in single-lap shear tests.

**Table 3.** Average strength and failure mode from pull-off tests (CoV within parentheses).

Specimens	Average strength [N/mm <sup>2</sup> ]	Failure mode
REF	1.41 (1.4%)	 Cohesive
SATU	1.33 (5.2%)	 Cohesive
POST	0.02 (20%)	 At the composite/brick interface

**Table 4.** Average strength of dry and saturated bricks (CoV within parentheses).

Test	Strength [N/mm <sup>2</sup> ]		Strength variation
	Dry	Saturated	
Three-point bending test	5.02 (17%)	4.05 (24%)	-20%
Tensile splitting test	4.67 (15%)	3.79 (10%)	-19%

To advance the knowledge about the tensile behavior of the brick in dry and saturated conditions, flexural and tensile splitting tests were carried out and Table 4 summarizes the strength values obtained for the specimens collected from two REF masonry blocks after the direct-shear tests were completed (Fig. 6). Outlier strength values were excluded. The average strength values obtained from the two tests are quite similar for dry and saturated conditions. The strength reduction associated with water saturation can be inferred from both tests and is about 20%. Such strength decrease of brick could be responsible for the reduction in bond strength found in the direct-shear and pull-off tests of

SATU specimens when compared with REF specimens. This aspect should be considered when SRP-reinforced masonry is subject to wetting by rain, rising damp from soil, or condensation.

#### **4. Conclusions**

In this paper, an experimental investigation was carried out to study the bond behavior of SRP-masonry joints under conditions typically found in masonry buildings, namely the deterioration by salts at the moment of the composite application and the presence of moisture in the substrate during the composite life span. To take into account these conditions, reference SRP-masonry joints (REF), saturated SRP-masonry joints (SATU) and SRP-masonry joints in which the composite was applied on salt-deteriorated blocks (POST) were subjected to single-lap shear tests. Digital image correlation was used to obtain the displacement and strain fields on the surface of the SRP strip during the whole stress-transfer process. After the shear tests were performed, the fracture surface was carefully observed and, for POST specimens only, the internal salt distribution was investigated by ion chromatography. Pull-off tests were also carried out on SRP-strengthened bricks in weathered, saturated, and dry conditions of the substrate, to correlate the results with the single-lap shear tests. Additional tests (three-point bending test and tensile splitting test) were used to compare the tensile behavior of brick in dry and water saturated conditions, as this aspect is expected to influence the bond behavior of SRP-masonry joints in wet conditions. From the results obtained, the following conclusions can be drawn:

- the majority of specimens exhibited a cohesive failure in direct-shear tests, involving the debonding of SRP strip with a layer of substrate attached. For saturated and weathered specimens (SATU and POST), the attached substrate layer was thinner with respect to control specimens, indicating a weaker bond;
- interlaminar failure was observed in some POST specimens tested in direct-shear tests, which can be attributed to a premature loss of viscosity of epoxy resin during casting leading

to some defects inside the composite matrix. This observation calls for further investigation to confirm the results;

- both in the shear tests and pull-off tests, the bond strength of water saturated (SATU) specimens was generally lower than that of REF specimens, because of the weaker mechanical properties of bricks in moist conditions, which were confirmed by additional flexural and indirect tensile tests comparing dry and saturated bricks (tensile strength decrease of about 20% was found between saturated and dry specimens);
- artificial weathering process by salt crystallization cycles altered the properties of the masonry surface (POST), leading to a potential change in the bond properties between the composite and substrate. When adhesion was tested perpendicularly to the brick/composite surface, i.e. in the pull-off test, the salt-deteriorated state of the brick led to a negligible adhesion, being the bonding strength almost zero ( $0.02 \text{ N/mm}^2$  on average). Conversely, in the direct-shear tests, the load response of specimens in which the SRP strip was bonded to salt-deteriorated masonry blocks (POST) was similar to that of REF specimens that did not undergo any weathering cycle. The failure mode of direct-shear POST specimens suggested the activation of multiple interfaces that was not observed for SATU and REF specimens. The cause behind this different interface activation could just be related to some issues with casting the POST specimens or might suggest an effect of salt hygroscopic behaviour on the polymerization of the epoxy;
- ion chromatography revealed an increase in the amount of chloride ions and sulfate ions for masonry blocks after artificial weathering. The amounts found beneath the surface of the composite can be considered similar to those found in historical buildings. However, the irregular salt distribution on the top surface of the masonry blocks might be one of the reasons for some scattering in the results of the single-lap shear tests.

## Acknowledgements

Technicians of LISG and LASTM laboratories (DICAM Department) and CIRI-EC of the University of Bologna, Mr. Giovanni Quartarone and Mr. Lorenzo Ferrari are gratefully acknowledged for their help during the experimental campaign. Kerakoll S.p.A. (Sassuolo, Italy) is acknowledged for providing the composite materials.

## References

- [1] Vaculik, J., Visintin, P., Burton, N. G., Griffith, M. C., Seracino. R., State-of-the-art review and future research directions for FRP-to-masonry bond research: Test methods and techniques for extraction of bond-slip behaviour. *Construction and Building Materials*, 2018. 183: p. 325-345.
- [2] Valluzzi, M.R., Modena, C., de Felice, G., Current practice and open issues in strengthening historical buildings with composites. *Materials and Structures/Materiaux et Constructions*, 2014. 47(12): p. 1971-1985.
- [3] De Santis, S., de Felice, G., Napoli, A., Realfonzo, R., Strengthening of structures with Steel Reinforced Polymers: A state-of-the-art review. *Composites Part B: Engineering*, 2016. 104: p. 87-110.
- [4] Sneed, L.H., Ravazdezh, F., Santandrea, M., Imohamed, A.O.I., Carloni C. (2017). A study of the compressive behavior of concrete columns confined with steel-FRP jackets using digital image analysis. *Composites Structures*, 179, 195–207.
- [5] Casadei, P., Nanni, A., Alkhrdaji, T. Steel-reinforced polymer: An innovative and promising material for strengthening infrastructures. *Concrete Engineering International*, 2005. 9 (1): p. 54-56
- [5] Ceroni, F., de Felice, G., Grande, E., *et al.*, Analytical and numerical modeling of composite-to-brick bond. *Materials and Structures/Materiaux et Constructions*, 2014. 47(12): p. 1987-2003.
- [7] de Felice, G., Aiello, M. A., Bellini, A., *et al.*, Experimental characterization of composite-to-brick masonry shear bond. *Materials and Structures/Materiaux et Constructions*, 2016. 49(7): p. 2581-2596.

- [8] Maljaee, H., Ghiassi, B., Lourenco, P. B., Oliveira, D. V., Moisture-induced degradation of interfacial bond in FRP-strengthened masonry. *Composites Part B: Engineering*, 2016. 87: p. 47-58.
- [9] Ghiassi, B., Marcari, G., Oliveira, D. V., Lourenço, P. B., Water degrading effects on the bond behavior in FRP-strengthened masonry. *Composites Part B: Engineering*, 2013. 54(1): p. 11-19.
- [10] Tedeschi, C., Kwiecien, A., Valluzzi, M. R., Zajac, B., Garbin, E., Binda, L., Effect of thermal ageing and salt decay on bond between FRP and masonry. *Materials and Structures/Materiaux et Constructions*, 2014. 47(12): p. 2051-2065.
- [11] Valluzzi M., Binda L., Tedeschi C., Garbin E., Panizza M., Salt crystallization test on brick masonry reinforced by CFRP textiles. In: 12<sup>th</sup> International Conference on Durability of Building Materials and Components, Porto, 2011.
- [12] Gentilini, C., Franzoni, E., Santandrea, M., Carloni, C., Salt-induced deterioration on FRP-brick masonry bond. In: Aguilar R., Torrealva D., Moreira S., Pando M.A., Ramos L.F. (eds) *Structural Analysis of Historical Constructions*. RILEM Bookseries, vol 18. Springer, Cham, 2019.
- [13] Capozucca, R., Experimental FRP/SRP-historic masonry delamination. *Composite Structures*, 2010. 92(4): p. 891-903.
- [14] Capozucca, R., Experimental analysis of historic masonry walls reinforced by CFRP under in-plane cyclic loading. *Composite Structures*, 2011. 94: p. 277-289.
- [15] Capozucca, R., Ricci, V., Bond of GFRP strips on modern and historic brickwork masonry. *Composite Structures*, 2016. 140: p. 540-555.
- [16] Franzoni, E., Santandrea, M., Gentilini, C., Fregni, A., Carloni, C., The role of mortar matrix in the bond behavior and salt crystallization resistance of FRCM applied to masonry. *Construction and Building Materials*, 2019. 209: p. 592-605.
- [17] Franzoni, C., Santandrea, M., Zanotto, S., Carloni, C., Durability of steel FRCM-masonry joints: effect of water and salt crystallization. *Materials and Structures*, 2017: p. 50:201.



- [18] Yuan, Y., Gentilini, C., Carloni, C., Franzoni, E., Adhesion between SRP and masonry: Influence of moist condition of specimens and presence of salts in the substrate. *Key Engineering Materials*, 2019. 817 KEM: p. 182-187.
- [19] EN 772-1 (2015), Methods of test for masonry units - Part 1: Determination of compressive strength.
- [20] EN 12390-6 (2009), Testing hardened concrete. Tensile splitting strength of test specimens.
- [21] EN 771-1:2011. Specification for masonry units. Clay masonry units length
- [22] EN 1052-3:2002. Methods of test for masonry — Part 3: Determination of initial shear strength
- [23] Sandrolini, F., Franzoni, E. An operative protocol for reliable measurements of moisture in porous materials of ancient buildings. *Building and Environment*, 2006. 41: p.1372–1380
- [24] Ucer, D., Ulybin, A., Zubkov, S., Elias-Ozkan, S.T. Analysis on the mechanical properties of historical brick masonry after machinery demolition. *Construction and Building Materials*, 2018. 161: p. 186-195
- [25] Ulukaya, S., Yoruç, A.B.H., Yüzer, N., Oktay, D. Material characterization of byzantine period brick masonry walls revealed in Istanbul (Turkey). *Periodica Polytechnica Civil Engineering*, 2017. 61 (2): p. 209-215
- [26] Foraboschi, P., Vanin, A. Experimental investigation on bricks from historical Venetian buildings subjected to moisture and salt crystallization. *Engineering Failure Analysis*, 2014. 45: p. 185–203.
- [27] Kamendere, E., Grava, L., Zvaigznitis, K., Kamenders, A., Blumberga, A. Properties of Bricks and Masonry of Historical Buildings as a Background for Safe Renovation Measures. *Energy Procedia*, 2016. 95: p. 119-123
- [28] Grande, E., Imbimbo, M., Sacco, E. Bond Behavior of Historical Clay Bricks Strengthened with Steel Reinforced Polymers (SRP). *Materials*, 2011. 4: p. 585-600

- [29] Baietti, G., Franzoni, E., Quartarone, G., Fregni, A., Carloni, C. Bond behavior between tuff and fired-clay brick masonry blocks and srg composites. *Key Engineering Materials*, 2019. 817 KEM: p. 118-125
- [30] Tang, Y., Yin, Q. A study of microproperties of historical brick material and qualitative correlation between strength and pore distribution. *Advanced Materials Research*, 2012. 450-451: p. 210-217
- [31] Mahasuwanchai, P., Wonganan, N., Athisakul, C., Tangchirapat, W., Sahamitmongkol, R., Leelataviwat, S. Engineering properties of ancient masonry materials in Thailand and substitution materials for historical structures preservation. *IOP Conference Series: Earth and Environmental Science*, 2020. 463 (1): art. no. 12077
- [32] Moropoulou, A., Polikreti, K. Principal Component Analysis in monument conservation: Three application examples. *Journal of Cultural Heritage*, 2009. 10 (1): p. 73-81
- [33] EN 998-2 (2016), Specification for mortar for masonry - Part 2: Masonry mortar.
- [34] Franzoni, E., Rising damp removal from historical masonries: a still open challenge. *Construction and Building Materials*, 2014. 54: p. 123–136.
- [35] Datasheets of GeoLite® Gel, Kerakoll S.p.A., Italy [November 2019].
- [36] Datasheets of GeoSteel G1200, Kerakoll S.p.A., Italy [November 2019].
- [37] Salsavilca, J., Yacila, J., Tarque, N., Camata, G. Experimental and analytical bond behaviour of masonry strengthened with steel reinforced grout (SRG). *Construction and Building Materials*, 2020. 238: p. 117635.
- [38] De Santis, S., Carozzi, F., De Felice, G., Poggi, C. Test methods for textile reinforced mortar systems. *Composites Part B: Engineering*, 2017b. 127: p. 121-132.
- [39] EN 1542:1999, Products and systems for the protection and repair of concrete structures — Testmethods — Measurement of bond strength by pull-off.
- [40] CNR-DT 200R1/2013, Guide for the design and construction of externally bonded FRP systems for strengthening existing structures, in Italian Research Council, Rome.

- [41] Sassoni, E., Andreotti, S., Bellini, A., Mazzanti, B., Bignozzi, M. C., Mazzotti, C., Franzoni, E., Influence of mechanical properties, anisotropy, surface roughness and porosity of brick on FRP debonding force. *Composites Part B: Engineering*, 2017. 108: p. 257-269.
- [42] Carrara, P., Ferretti, D., Freddi, F., Rosati, G., Shear tests of carbon fiber plates bonded to concrete with control of snap-back. *Engineering Fracture Mechanics*, 2011. 78(15): p. 2663-2678.
- [43] Carrara, P., Ferretti, D., A finite-difference model with mixed interface laws for shear tests of FRP plates bonded to concrete. *Composites Part B: Engineering*, 2013. 54: p. 329-342.
- [44] Carloni, C., Subramaniam, K.V., FRP-masonry debonding: Numerical and experimental study of the role of mortar joints. *Journal of Composites for Construction*, 2012. 16(5): p. 581-589.
- [45] Carloni, C., Focacci, F., FRP-masonry interfacial debonding: An energy balance approach to determine the influence of the mortar joints. *European Journal of Mechanics A/Solids*, 2016. 55: P. 122-133.
- [46] Focacci, F., Carloni, C., Periodic variation of the transferable load at the FRP-masonry interface. *Composite Structures*, 2015. 129: p. 90-100.
- [47] Napoli, A., de Felice, G., De Santis, S., Realfonzo, R., Bond behaviour of Steel Reinforced Polymer strengthening systems. *Composite Structures*, 2016. 152: p. 499-515.
- [48] Dai, J., Ueda, T., Sato, Y., Development of the nonlinear bond stress-slip model of fiber reinforced plastics sheet-concrete interfaces with a simple method. *Journal of Composites for Construction*, 2005. 9(1): p. 52-62.
- [49] Carloni, C., Imohamed, I. A. O., Santandrea, M., Determination of the interfacial properties of SRP strips bonded to concrete and comparison between single-lap and notched beam tests. *Engineering Fracture Mechanics*, 2017. 186: p. 80-104.
- [50] Sandrolini, F., Franzoni, E., Cuppini, G., Caggiati, L., Materials decay and environmental attack in the Pio Palace at Carpi: A holistic approach for historical architectural surfaces conservation. *Building and Environment*, 2007. 42(5): p. 1966-1974.

[51] Sandrolini, F., Franzoni, E., Characterization procedure for ancient mortars' restoration: The plasters of the Cavallerizza courtyard in the Ducal Palace in Mantua (Italy). *Materials Characterization*, 2010. 61(1): p. 97-104.